A Kinetic Energy Budget of a Subtropical Prefrontal Rainband Based on Dual-Doppler Measurements

YEONG-JER LIN[1], HSIU-WU CHANG[1,3] and ROBERT W. PASKEN[2]

ABSTRACT

Dual-Doppler data collected during the Taiwan Area Mesoscale Experiment (TAMEX) were used to study the kinetic energy balance of a subtropical prefrontal rainband over the Taiwan Strait. Fields of the system-relative wind and reflectivity were derived in a horizontal domain of 36 km by 40 km using the objective analysis scheme with 1-km grid spacing in all three directions, except in the lowest two levels where the height increment was chosen to be 0.5 km. There were ten analysis levels in the vertical ranging from 0.4 to 8.8 km. Vertical velocities were computed from the anelastic continuity equation by integrating downward with variational adjustment. Subsequently, fields of perturbation pressure and temperature were retrieved from a detailed wind field using the three momentum equations.

The Doppler-derived winds and retrieved thermodynamic variables are then used to compute the magnitude of each term in the kinetic energy budget equation. Results show that the vertical total of the horizontal generation term acts as the main source of kinetic energy, while vertical totals of dissipation and the horizontal flux convergence/divergence of kinetic energy provide the main sinks. The horizontal flux convergence/divergence of kinetic energy is nearly balanced by the vertical flux convergence/divergence at most levels. In a similar manner, the vertical generation of kinetic energy term is almost in balance with the total buoyancy term. The computed tendencies show the decrease of mean kinetic energy at low levels and the increase at middle levels, which are attributable to the generation and redistribution of kinetic energy and latent heat releases by organized convection associated with the rainband. These findings are consistent with the weakening of a low-level jet and the formation of a middle-level jet at the times of convection as revealed by upper air observations. The budget study further demonstrates that the storm's meso-γ-scale environment is modified by areas of convection through scale interaction or "feedback" mechanisms.

---

[1] Department of Earth and Atmospheric Sciences, Saint Louis University, St. Louis, Missouri, U.S.A.

[2] Department of Science and Mathematics, Parks College of Saint Louis University, Cahokia, Illinois, U.S.A.

[3] Present affiliation: Central Weather Bureau, Taipei, Taiwan, R.O.C.

1. INTRODUCTION

It is well documented that atmospheric processes are characterized by various scales of motion, ranging from large-scale, meso-scale, to small-scale turbulent eddies. Observational evidence has revealed that non-linear scale interactions are mainly responsible for transferring kinetic energy (KE) from one scale to another. Mesoscale phenomena, e.g., convective storms and squall lines, are affected by both larger and smaller scale eddies. During the developing and mature stages of these mesoscale disturbances, the large-scale environments are considerably modified as a result of scale interactions or *"feedback"* mechanisms. These dynamic interactions are very complicated in nature and have not been well understood, yet. One way of investigating these feedback processes is to examine the KE balance of the storm's surroundings, e.g., Fuelberg and Printy (1984), etc.

Case studies by Ninomiya (1971), Maddox (1980), and many others have shown that storm-environment interactions result in a mid-tropospheric warming and ascent, strong low-level convergence and upper-level divergence, regions of upper-level ridging and anticyclonic flow, and the formation of jet maxima on their poleward sides in the storm's surroundings. Additionally, mesoscale investigations of storm-environment interaction by Ogura and Chen (1977), Sanders and Emanuel (1977), Ogura and Liou (1980), Vincent and Carney (1982), Fuelberg and Jedlovec (1982), etc. have confirmed the findings that were observed at the synoptic scale. Nevertheless, more detailed studies are needed in order to better understand the physical mechanisms involved.

Unlike the synoptic and mesoscale case studies mentioned previously , there are very few observational studies in the literature that describe the effects of convection on its meso-γ-scale environment. Using the dual-Doppler data collected during JAWS (Joint Airport Weather Studies), Lin and Coover (1988) conducted a KE analysis of a microburst-producing thunderstorm with 0.5-km grid spacing. Lin *et al.* (1991) studied the KE budget of a subtropical squall line over the Taiwan Strait based on the dual-Doppler measurements during the project of TAMEX (Taiwan Area Mesoscale Experiment). Results showed that vertical totals of the horizontal generation and total buoyancy production terms acted as a source of KE, while vertical totals of dissipation and vertical generation provided the main sinks. The horizontal flux convergence (divergence) of KE was nearly balanced by the vertical flux divergence (convergence) at most levels. The vertical total of KE change was negative for both the observed and computed values, showing the decrease of total KE of the squall system as it approached the west coast of Taiwan.

The purpose of this study was to conduct a KE budget study of a subtropical convective rainband as it approached the northwest coast of Taiwan. The KE budgets are assessed over the horizontal domain of 25 $\times$ 40 km^2 covering the convective and stratiform regions. The important physical processes contributing to the KE budget are investigated in detail. In particular, the interaction of energy-generating processes with their meso-γ-scale environment can be better understood by using the KE budget equation. Further, such a budget study can lead us to a better understanding of how areas of organized convection modify their larger scale surroundings in the subtropical environment. It facilitates direct comparisons with the previous meso-γ-scale KE analysis during TAMEX IOP 2 (Lin *et al.*, 1991) and other mesoscale KE analyses reported. The goal is to gain a better understanding on how the convective rainband modifies the wind and thermal structure of its surrounding environment through scale interaction.

2. DATA AND METHODOLOGY

In turbulent theory, scale interaction means the numerous interactions in a continuous spectrum of eddies of all sizes. Factual evidence reveals that on the average the mesoscale is much like a continuous spectrum of scale. In reality, the spectrum of atmospheric motions is smooth and continuous between the limits imposed by the mean free path of the molecules on the short end and the circumference of the earth on the large (Emanuel, 1986).

The non-linear dynamical equations of motion contain information about atmospheric motion and transport over a broad range of spatial scales, ranging from large-scale to small-scale turbulent eddies. However, only the statistical properties of the turbulent eddies can be properly described, and an average operator must be introduced to obtain the statistical mean (Cotton and Anthes, 1989).

Anthes (1977) introduced several methods of averaging the dynamical equations. For a smaller domain in which clouds comprise 50 to 100% coverage of the domain the classical Reynolds averaging method, by considering the convective clouds as eddies superimposed on a larger scale flow, becomes more suitable.

This study is an extension of the study by Lin *et al.* (1992). Dual-Doppler data from the CP-4 and TOGA radars at 0653 and 0700 LST (local standard time) 25 June 1987 during TAMEX were used to investigate the structure and internal dynamics of a subtropical prefrontal convective rainband. These data were objectively analyzed onto the horizontal Cartesian grids (36 km × 40 km) at each analysis level using a 1-km grid spacing in all three directions . The *"resolvable"* scale (one-half wavelength) in this study is 3 km or greater. It follows that features associated with large-scale, meso-α-scale, meso-β-scale and meso-γ-scale (Orlanski, 1975) are adequately resolved in the current study. These features were presented at ten analysis levels from 0.4 to 8.8 km. Because of the lack of *"good"* data (i. e., high signal-to-noise ratio data), in the upper troposphere, analyses were confined to those levels below 9 km. However, in the calculation of vertical velocity, the storm top is assumed to be at 11 km.

Vertical velocities were computed from the anelastic continuity equation by integrating downward from the storm top with variational adjustment. Subsequently, fields of deviation perturbation pressure and virtual temperature were retrieved from the Doppler-derived winds using the three momentum equation, e.g., Gal-Chen (1978), etc.

Following the study by Lin and Coover (1988), the KE equation for a nonhydrostatic system can be written as

$$\underbrace{\left\{ \frac{\partial \rho_o K_3}{\partial t} \right\}}_{\text{LTK}} = - \underbrace{\left\{ \nabla_h \cdot \left(\rho_o K_3 V_h \right) \right\}}_{\text{HFD}} - \underbrace{\left\{ \frac{\partial \rho_o K_3 w}{\partial z} \right\}}_{\text{VFD}}$$

$$- \underbrace{\left\{ V_h \cdot \nabla_h P' \right\}}_{\text{HGE}} - \underbrace{\left\{ w \frac{\partial P'}{\partial z} \right\}}_{\text{VGE}}$$

$$+ \underbrace{\left\{ \rho_o g w \left(\frac{T'_v}{T_{vo}} - q_t \right) \right\}}_{\text{BUP}} + \underbrace{\left\{ \rho_o V \cdot F \right\}}_{\text{FDI}} , \qquad (1)$$

where $\{(\ \ )\} = (1/area) \int \int (\ \ ) \, dxdy$, $K_3 = (u^2 + v^2 + w^2)/2$ is the total KE per unit mass, the subscript 0 represents the environmental mean, the prime denotes the deviation from the environmental mean, and the other symbols have their conventional meanings. Notice that the horizontal domain with dimensions of 25 km by 40 km was employed to obtain the area mean of each quantity in the KE budget equation (1). This mean quantity represents the averaged property obtained in the meso-γ-scale environment in relation to the convective-scale eddies embedded within the system.

Terms on the right-hand side of (1) represent the horizontal flux divergence (HFD), the vertical flux divergence (VFD), the horizontal generation (HGE), the vertical generation (VGE), the total buoyancy production (BUP), and the frictional dissipation (FDI) of KE, respectively. Physically speaking, the horizontal and vertical flux divergence terms (HFD and VFD) represent the interaction between the convective-scale eddies, embedded within the rainband, and their meso-γ-scale surroundings. These two terms do not generate KE, but rather redistribute KE within the system and transfer it from one scale to another. The generation terms (HGE and VGE) denote the generation of KE, or conversion of potential energy (PE) to KE, by ageostrophic flow. If the wind blows from high pressure to low pressure (downgradient), KE will be gained as a result of mechanical work done by the pressure gradient force. Conversely, if the flow blows from low pressure to high pressure (countergradient), then KE will be lost or converted to PE. The total buoyancy production term (BUP) is composed of the contributions of thermal buoyancy (BUO) and precipitation loading. Values of BUO are positive when the warm air rises, due to latent heat releases by condensation, and cold air descends, due to the combined effects of evaporative cooling and precipitation loading. Finally, the frictional dissipation term (FDI) shows the dissipation of KE by subgrid-scale (*" unresolvable"* scale) processes.

3. DISCUSSION OF RESULTS

Two volumes of dual-Doppler data at 0653 and 0700 LST 25 June were considered in this study. At the times of analysis, the system traveled from $330°$ at 2.5 ms^{-1}. This speed was much slower than that reported in studies by Carbone (1982) and Lin *et al.* (1990).

3.1 Rainband Characteristics

Some structural features of the prefrontal rainband under investigation were detailed in studies by Lin *et al.* (1992) and Lin *et al.* (1993). This rainband developed on the warm side of the Mei-Yu front over northwestern Taiwan as the front was approaching the northwest coast. The southwesterly monsoon flow in the warm sector was accompanied by a low-level jet (LLJ) near the 900 mb level. The cold front provided large-scale lifting in the boundary layer to initiate organized convection along the front. In the middle and upper troposphere, the reflectivity core associated with the frontal updraft was elongated toward the southeast in the direction of the environmental shear. This reflectivity core induced a weak convective downdraft ahead of the surface front due largely to precipitation loading. The descending air of the downdraft resulted in cool diverging outflows in the boundary layer, triggering new convection on the southeast side of the rainband. The prefrontal rainband traveled slowly south-southeastward at 2.5 ms^{-1}, and consisted of many cells in a narrow band. Each cell was accompanied by the moderate convective updraft and downdraft. The rainband produced heavy precipitation on the west coast of Taiwan.

Figure 1 shows fields of the horizontal system relative wind, with reflectivity contours superimposed, and horizontal divergence at 0653 LST for 0.35 km. A distinct line of wind-shift (heavy broken line) is seen (Figure 1a). This line matches well with the position of the Mei-Yu front and exhibits a wavy pattern, showingthe mesoscale structure (Lin *et al.*, 1992). The position of the wind-shift line coincides with the zone of horizontal convergence (Figure 1b). On the left side of the wind-shift line, the winds are predominantly from the northwest, transporting cooler, drier air from northern China to the Taiwan Strait. Conversely, the southwest monsoon prevails in the warm sector to the southeast of the wind-shift line. It transports high-θ_e air from the South China Sea to the Mei-Yu front. Such air feeds the convective updrafts, resulting in a widespread area of upward motion in the vicinity of the wind-shift line (see areas of convergence in Figure 1b). Conversely, downward motion dominates in a broad area southeast of the wind-shift line. Such downward motion is associated with the precipitation-induced convective downdrafts in the warm sector (Lin *et al.*, 1992 and Lin *et al.*, 1993). These convective downdrafts (see areas of divergence in Figure 1b) generate cold outflows in the boundary layer. Part of these cold outflows moves toward the southeast, interacting with incoming high-θ_e air from the southwest to form a gust front (dotted line). This gust front indicates the leading edge of the rainband. It is characterized by low-level convergence, upward motion, high reflectivity, and slight wind shift.

Figure 2 displays the system-relative wind with reflectivity contours superimposed at 0653 LST for 2.75 km. The box in the figure signifies the horizontal domain used for budget calculation. The approximate position of the surface cold front (heavy broken line) is indicated in Figure 2b. Notice that upward motion (hatched) dominates in a broad area along the surface front with a maximum of 8-9 ms^{-1} due largely to frontal lifting in the boundary layer. In a similar manner, upward motion also prevails in the areas along the surface gust front (dotted line) on the southeast side of the front. The reflectivity cores (shaded) associated with the frontal updrafts are tilted toward the southeast (right side of Figure 2) with the shear. Convective downdrafts form in the high reflectivity regions due to precipitation loading. As noted earlier, these downdrafts carry much cooler air downward, resulting in cold outflows at low levels (Lin *et al.*, 1993). Part of these cold outflows interacts with the high-θ_e monsoon flow to initiate new convection along the gust front (dotted line). New cells move toward the east-northeast at higher speeds (6-7 ms^{-1}) following the prevailing flow in the warm sector. These new cells eventually merge with the old cells to maintain the lifetime of the rainband (Lin *et al.*, 1992).

3.2 Kinetic Energy Budget

Budgets of the total KE, per unit volume, were calculated from (1) by integrating over a 25 × 40 km^2 horizontal domain at each level. Figure 3 shows vertical profiles of the horizontal flux convergence (HFD) and the vertical flux convergence (VFD) of KE in units of 10^{-3} W m^{-3}. A positive value indicates the flux convergence and vice-versa. Note that the HFD term is positive (flux convergence) at heights below 4.5 km and is negative (flux divergence) higher up. Conversely, values of VFD are negative at levels below 4 km and positive aloft. These two terms have the same order of magnitude, but opposite signs at most levels. The total flux term (TFD) represents the three-dimensional distribution of the flux convergence/divergence of KE due to storm-environment interactions. A positive value of TFD shows an increase in mean KE through *"feedback"* mechanisms by redistributing KE within the system and transferring it from convective-scale eddies to their meso-γ-scale
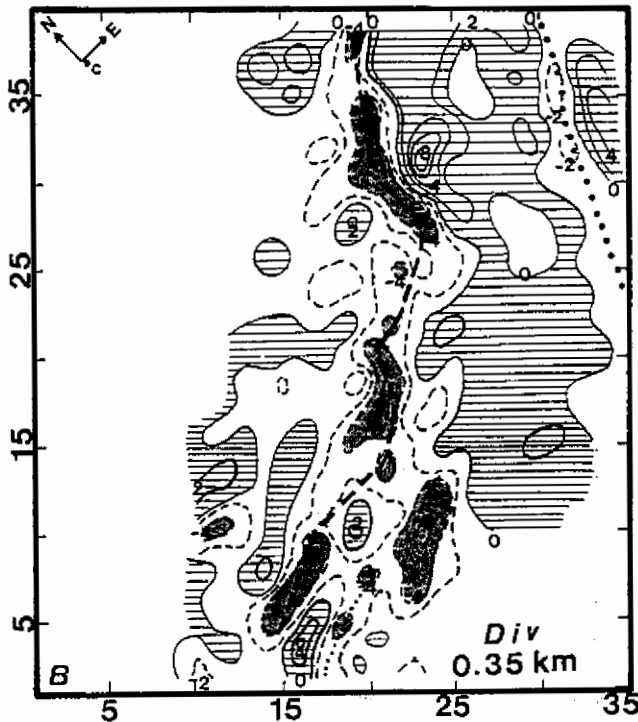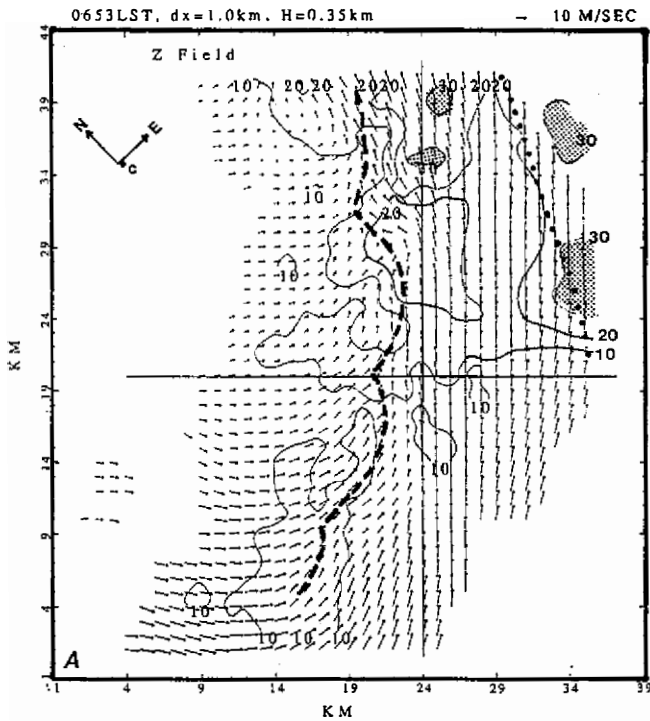
Fig. 1. Horizontal distributions of the (a) system-relative wind with reflectivity contours (Z) superimposed, and (b) horizontal convergence/divergence at 0.35 km for 0653 LST 25 June 1987. The heavy-broken line shows the wind-shift line, while the dotted line denotes a gust front. Contour interval for convergence/divergence is $2 \times 10^{-3} s^{-1}$ with positive values (divergences) hatched. The shaded area shows convergences $> -4 \times 10^{-3} s^{-1}$.
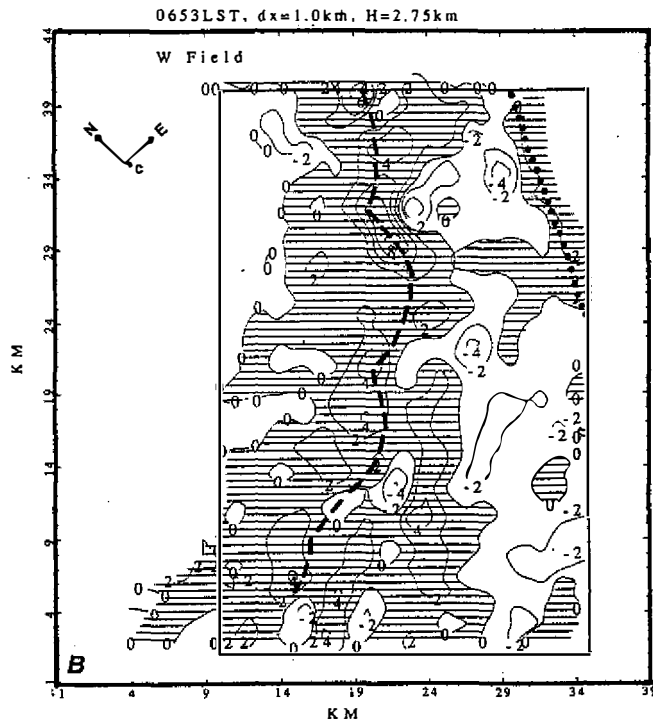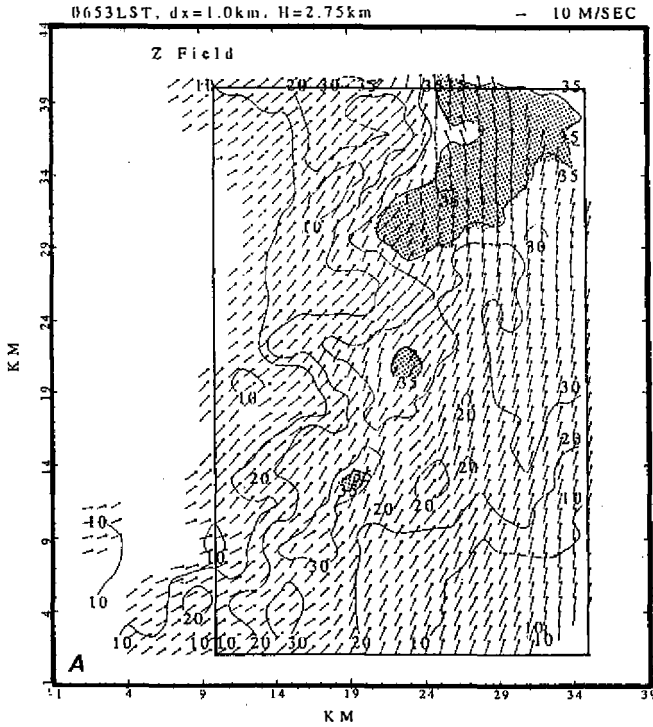
Fig. 2. Horizontal distributions of the (a) system-relative wind with reflectivity contours (Z) superimposed, and (b) vertical velocity (w) at 2.75 km for 0653 LST 25 June 1987. Contour interval for w is 2 ms^{-1} with positive values hatched. Reflectivities > 30 dBZ are shaded. North (N), east (E), and system motion (C) are indicated in panel b.

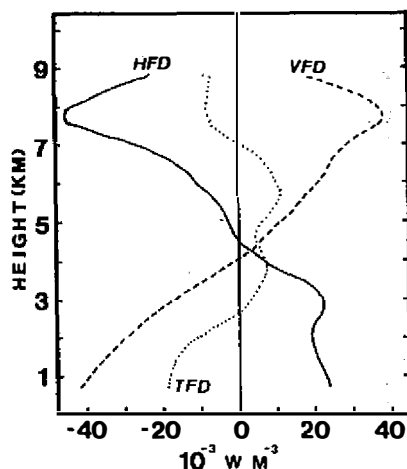*Fig. 3.* Vertical profiles of the horizontal flux divergence (HFD), vertical flux divergence (VFD), and total flux divergence (TFD) of kinetic energy. The vertical axis shows heights in kilometers above the sea level. Units are in $10^{-3} \mathrm{W} \, m^{-3}$.

surroundings. The reverse is true for a negative value of TFD. Notice that values of TFD are negative in the lower and upper layers and positive in the middle layer, showing a net gain of KE in the layer between 3 and 7 km with a net loss in the layers above and below. The mean vertical transport of KE, $\rho_o K_3 W$, by organized convection is predominantly positive from the surface to 8.5 km with the maximum ($10^2 \mathrm{W} \, m^{-2}$) occurring in the 3-4 km layer (Figure 4). This finding clearly shows that the mean KE in the meso-γ-scale surroundings is substantially increased in the middle troposphere at the times of convection due to storm-environment interactions mentioned previously. As stated in Lin *et al.* (1993), the frontal lifting in the boundary layer together with positive buoyancy aloft are responsible for an upward transport of kinetic energy.

Vertical variations of VGE and BUP are illustrated in Figure 5. For comparison, the TFD term discussed previously is also displayed. Notice that magnitudes of VGE and BUP are much smaller than those of HFD and VFD (Figure 3) at most levels. The VGE term has negative values at heights below 4.5 km with positive values aloft. The total buoyancy term (BUP) is nearly balanced by the vertical generation term (VGE) at most levels. The BUP term consists of the contributions of thermal buoyancy (BUO) and precipitation loading. The latter normally has a negative contribution to BUP, while the former can either be positive or negative. Values of BUO are positive when warm air rises and cold air descends. Conversely, BUO becomes negative when warm air is forced to descend and cold air is lifted upward. Notice that values of BUP are positive in the layer below 4 km. In this layer, the warm air ascends within the convective updraft, due to the latent heat release by condensation, resulting in a gain of KE over that layer. In the same layer, the cool air descends within the convective downdrafts, due to evaporative cooling and rain loading, resulting in a positive generation of BUP. Values of BUP become negative in the layer above 4 km. In this layer, the precipitation loading term overcomes the BUO term, hence values of BUP become negative. Figure 6 shows vertical variations of the HGE and FDI terms. Values of HGE are positive at most levels with a maximum near 2.5 km. A positive value of HGE occurs when the wind blows from high pressure to low pressure. The frictional term (FDI) is calculated from the momentum fluxes and Doppler-derived winds. Its magnitude is relatively small in comparison with the other terms in (1). Negative values of FDI dominate throughout the troposphere, indicating a sink of KE at every level.
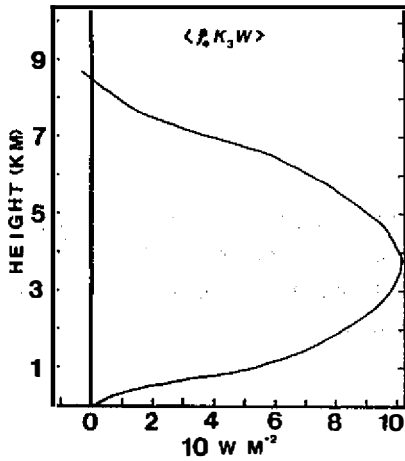
Fig. 4. The vertical distribution of mean vertical kinetic energy transport. Units are in watts per square meter (W m^{-2}).
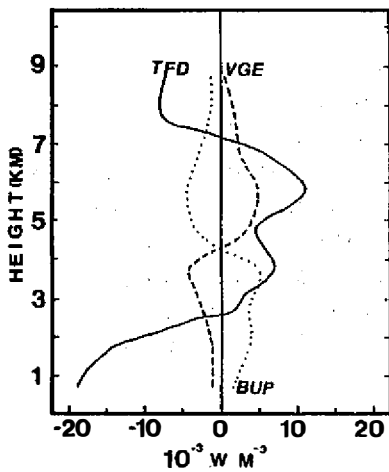

Fig. 5. As in Figure 3 except for the vertical generation (VGE), and total buoyancy (BUP) of kinetic energy,

The computed tendency (LTK) is obtained from (1) as a residual. This term should equal the sum of the net generation/dissipation inside the mesoscale domain and the net flux through the lateral analysis domain boundaries. Because of the uncertainty in wind, pressure, and temperature estimates (Lin *et al.*, 1991), the tendency term must be interpreted with caution. Note that values of LTK are negative in the layers below 2.5 km and above 7 km, and positive in the layer between 2.5 and 7 km (Figure 6). This finding shows that there is a net increase in KE in the middle troposphere, and a net decrease in the lower and upper troposphere. It is in qualitative agreement with the observation. As depicted in the study by Lin *et al.* (1992), the observed environmental winds significantly increased in the middle troposphere and decreased in the lower troposphere at the times of convection. As a result of organized convection associated with the rainband being investigated, the middle-level jet (MLJ) with a maximum of 23-25 ms^{-1} formed in the 600-400 mb layer, and the preexisting LLJ reduced in intensity considerably (Figure 7). According to Lin *et al.* (1993), the flux divergence of the vertical transport of horizontal momentum in the lower troposphere with the flux convergence in the middle troposphere were largely responsible for the generation
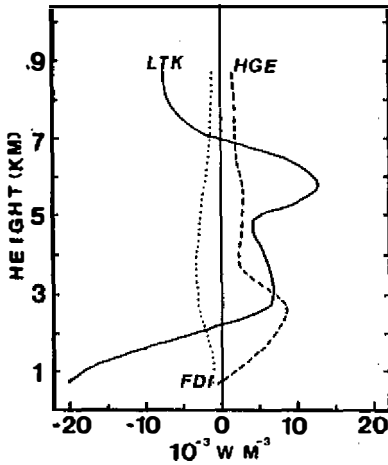
Fig. 6. As in Figure 3, except for the horizontal generation (HGE), frictional dissipation (FDI), and local time change of kinetic energy (LTK), units are in 10^{-3}W m^{-3}.
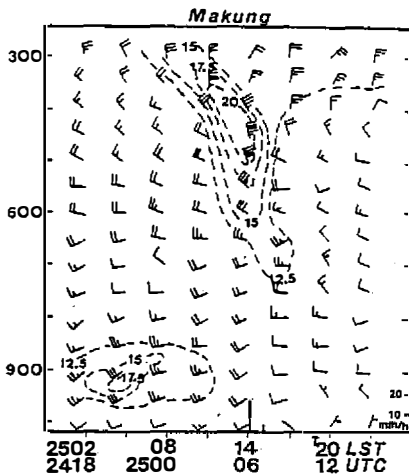

Fig. 7. Time-height variations of rawinsonde at Makung on 24-25 June 1987. The broken line represents an isotach in units of meters per second (ms^{-1}). The arrow shows the time of frontal passage. The vertical solid bar along the time axis shows the precipitation rate (mm h^{-1}). Adapted from Lin *et al.* (1992).

and dissipation of mean momentum observed.

The aforementioned result for LTK is significant, since it can explain the formation of an MLJ and the demise of an LLJ at the times of organized convection (Figure 7). It strongly suggests that the dynamical interaction between the convective rainband, embedded within the MCS, and its meso-γ-scale surroundings can lead to the generation and redistribution of mean KE. For example, in the 4-7 km layer (see Figure 6), LTK is of the order of 6×10^{-3} W m^{-3}. This is equivalent to the growth of mean KE at the rate of approximately 25 m^2 s-2 h-1 in the middle troposphere in qualitative agreement with the upper air observations taken at the Makung station in the strait (Figure 7). The result implies that an MLJ can form through scale interaction between convective-scale eddies within the system and their immediate surroundings at the times of organized convection. The result further shows that the relevant physical processes responsible for forming an MLJ are the generation and redistribution of KE and release of latent heat by condensation by the convective system.

In a similar manner, a decrease in mean KE in the lower troposphere is largely attributed to the redistribution of KE and transfer of KE from one scale to another through scale

interaction mentioned before. Notice that the decrease in mean KE is nearly offset by the increase at midlevels (see Figure 6 for comparison). It demonstrates that the strong KE associated with an LLJ is being transported upward (Figure 4) to develop an MLJ at the times of intense convection. In other words, both the mean horizontal momentum and KE in the immediate environment of the convective system can be effectively redistributed and transferred through scale interaction as a result of organized convection. Consequently, an MLJ formed and an LLJ weakened as supported by the upper air data (Figure 7).

3.3 Vertical Totals of Kinetic Energy

Table 1 presents budgets of the total KE averaged over a 25 × 40 km² horizontal domain and integrated over a depth of 1 km. Note that terms HFD and VFD have the same order of magnitude but opposite signs at most levels. Magnitudes of these two terms are much larger than the other terms in (1), especially in the lower and upper layers. The horizontal generation term (HGE) is positive at all levels, showing a net gain of kinetic energy. Like the flux terms, the vertical generation term is nearly balanced by the total buoyancy production term at most levels. On the other hand, the frictional dissipation term contributes negatively to the growth/decay of KE at every level. The computed tendency shows the increase of KE with time in the middle layer (2-7 km), and the decrease in the lower and upper layers.

Table 1. Kinetic energy budgets, averaged over a 25×40 km² horizontal domain and integrated over a depth of 1 km, at 0653 LST 25 June 1987. Units are in watts per square meter(Wm⁻²).

Layer (km)	HFD	VFD	TFD	HGE	VGE	BUP	FDI	LTK
8-9	-25.58	18.40	-7.18	1.55	0.45	-1.56	-0.82	-7.56
7-8	-45.98	38.18	-7.80	1.68	1.58	-1.68	-1.02	-7.24
6-7	-20.29	25.53	5.24	1.91	2.09	-2.96	-1.43	4.85
5-6	-6.74	18.58	11.84	2.67	4.93	-4.52	-1.77	13.15
4-5	-2.44	6.55	4.11	2.72	3.14	-3.27	-2.37	4.33
3-4	12.85	-5.90	6.95	2.16	-4.52	4.62	-2.55	6.66
2-3	21.75	-21.30	0.45	8.36	-2.66	3.20	-2.48	6.87
1-2	18.28	-33.06	-14.78	6.03	-1.17	3.61	-1.32	-7.63
SfC-1	23.21	-42.21	-19.00	-0.41	-1.14	1.51	-0.81	-19.85
Vertical Total	-24.94	4.77	-20.17	26.67	2.70	-1.05	-14.57	-6.42

The vertical total in Table 1 presents the total budget of each term from the surface to 9 km. Results show that terms HFD (-24.9 W m^{-2}) and FDI (-14.5 W m^{-2}) act as the main sinks of KE. Similarly, term BUP (-1.0 W m^{-2}) is a sink of KE. On the other hand, terms HGE (26.6 W m^{-2}), VFD (4.7 W m^{-2}), and VGE (2.7 W m^{-2}) are sources of KE. The vertical total for LTK is -6.4 W m^{-2}, showing a net decrease of total KE within the rainband at the times of investigation.

4. CONCLUSIONS

The Doppler-derived winds and retrieved thermodynamic variables on 25 June 1987 during TAMEX were used to investigate the KE balance of a subtropical prefrontal rainband over the Taiwan Strait. Results show that convective-scale eddies within the system effectively redistribute and transfer KE from one layer to another. The dynamical interactions between the convective-scale eddies and their meso-γ-scale surroundings result in a formation of an MLJ and a demise of an LLJ at the times of intense convection in agreement with observation. A KE budget study reveals that the horizontal and vertical flux divergence terms are dominant over the other terms in the budget equation. These two terms have the same order of magnitude, but opposite signs at most levels. Sources of KE come from the terms of horizontal generation, vertical generation and vertical flux convergence of KE, while the horizontal flux divergence, total buoyancy production and frictional dissipation terms are sinks of KE. The vertical total of KE change is negative, indicating the decrease of KE within the rainband at the times of analysis.

REFERENCES

Anthes, R. A., 1977: A cumulus parameterization scheme utilizing a one-dimensional cloud model. *Mon. Wea. Rev.*, **105**, 270-286.

Carbone, R., 1982: A severe frontal rainband. Part I: Storm-wide hydrodynamic structure. *J. Atmos. Sci.*, **39**, 258-279.

Cotton, W. R., and R. A. Anthes, 1989: Storm and cloud dynamics. International Geophysics Series, Academic Press, **44**, 883 pp.

Emanuel, K. A., 1986: Overview and definition of mesoscale meteorology in Mesoscale Meteorology and Forecasting, P. S. Ray, Ed., Amer. Meteor. Soc., 1-17.

Fuelberg, H. E., and G. J. Jedlovec, 1982: A subsynoptic-scale kinetic analysis of the Red River Valley tornado outbreak (AVE-SESAME I). *Mon. Wea. Rev.*, **110**, 2005-2029.

Fuelberg, H. E., and M. F. Printy, 1984: A kinetic energy analysis of the meso-β-scale severe storm environment. *J. Atmos. Sci.*, **41**, 3212-3226.

Gal-Chen, T., 1978: A method for the initialization of the anelastic equations. Implications for matching models with observations. *Mon. Wea. Rev.*, **106**, 587-606.

Lin, Y. J., and J. A. Coover, 1988: A kinetic energy analysis of a microburst-producing thunderstorm based on JAWS dual-Doppler data. *J. Atmos. Sci.*, **45**, 2764-2771.

Lin, Y. J., T. C. Wang, R. W. Pasken, H. Shen, and Z. S. Deng, 1990: Characteristics of a subtropical squall line determined from TAMEX dual-Doppler data. Part II: Dynamic and thermodynamic structures and momentum budgets. *J. Atmos. Sci.*, **47**, 2382-239

Lin, Y. J., H. Shen, and R. W. Pasken, 1991: Kinetic energy budgets of a subtropical squall line determined from TAMEX dual-Doppler measurements. *Mon. Wea. Rev.*, **119**, 2654-2663.

Lin, Y. J., R. W. Pasken, and H. W. Chang, 1992: The structure of a subtropical prefrontal convective rainband. Part I: Mesoscale kinematic structure determined from dual-Doppler measurements. *Mon. Wea. Rev.*, **120**, 1816-1836.

Lin, Y. J., H. W. Chang, and R. W. Pasken, 1993: The structure of a subtropical prefrontal convective rainband. Part II: Dynamic and thermodynamic structures and momentum budgets. *Mon. Wea. Rev.*, **121**, 1671-1687.

Maddox, R. A., 1980: Mesoscale convective complexes. *Bull. Amer. Meteor. Soc.*, **61**, 1374-1387.

Ninomiya, K., 1971: Mesoscale modification of synoptic situations from thunderstorms as revealed by ATS III and aerological data. *J. Appl. Meteor.*, **10**, 1103-1121.

Ogura, Y., and Y. Chen, 1977: A life history of an intense mesoscale convective storm in Oklahoma. *J. Atmos. Sci.*, **34**, 1458-1476.

Ogura, Y., and M. T. Liou, 1980: The structure of a midlatitude squall line. A case study. *J. Atmos. Sci.*, **37**, 553-567.

Orlanski, I., 1975: A national subdivision of scales for atmospheric processes. *Bull. Amer. Meteor. Soc.*, **56**, 527-530.

Sanders, F., and K. A. Emanuel, 1977: The momentum budget and temporal evolution of a mesoscale convective system. *J. Atmos. Sci.*, **34**, 322-330.

Vincent, D. G., and T. Q. Carney, 1982: Meso-synoptic scale circulation pattern during severe weather outbreak of April 10-11, 1979. Preprints 12th Conference on Severe Local Storms, San Antonio, Amer. Meteor. Soc., 556-559.